Terrestrial Planet Finder Coronagraph Status and Enabling Technologies

Mrs. Virginia G. Ford [*], Mr. Douglas Lisman, Dr. Stuart B Shaklan, Mr. Timothy Y. Ho, Mr. Andrew Kissil, Mr. Eug-Yun Kwack, Dr. Andrew Lowman

Jet Propulsion Laboratory, 4800 Oak Grove Drive, Pasadena, California, 91109-8099, USA

The goal of the Terrestrial Planet Finder Project Mission is to find life–bearing planets around nearby stars. Two types of instruments are competing for flight in 2015: a visible coronagraph and an infrared interferometer. The selected architecture must demonstrate that it is technically capable of detecting and spectrally characterizing earth-like planets around other stars. This presentation will cover an overview of the project, activities of the coronagraph team, describe the status and performance predictions of the coronagraph system, and discuss the technologies needed to perform this task. The technologies that will be covered relate to: system performance modeling; wave front sensing and control; optical element positioning; mask and stop fabrication, characterization, and tolerances; thermal control; and dynamics and pointing control. Up-to-date modeling results and test bed performance will be presented.

Nomenclature

AU	=	Astronomical Unit – orbital radius of Earth
TPF	=	Terrestrial Planet Finder
HST	=	Hubble Space Telescope
HCIT	=	High Contrast Imaging Testbed

I. Introduction

Since the mid 1980s dust disks around distant stars have been observed. Swirls and clear features in the observed disks indicate the presence of planets. Also, during the past 4 years, Astronomers using ground-based telescopes have been detecting many planets orbiting around nearby stars. The method used for this detection, called radial velocity detection, is to sense the Doppler-effect color shifting caused by the star wobble as the planet pulls on the star it orbits. Using this method, the planet's orbital radius and period and the planet's mass can be derived. This technique is optimized for sensing fast moving, heavy planets such as gas giants with very short orbital periods. This is because the fast moving, heavy planets displace the star more quickly with larger amplitude – both effects increase the Doppler shift of star light. As shown on Fig. 1, many more large planets with orbits
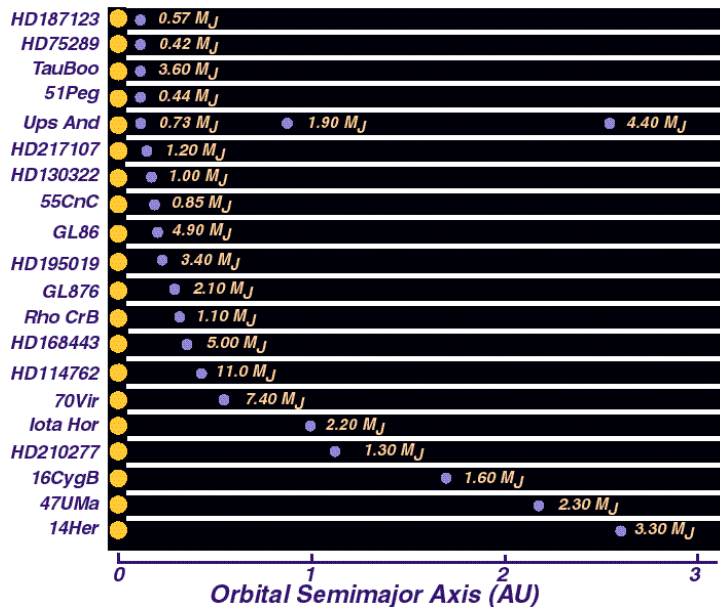

Figure 1. Discovery of planets around other stars.

---

extremely close to their stars have been detected than planets like our Jupiter with an orbital radius approximately 5 times larger than Earth.

The Radial Velocity measurements have found that about 10% of the observed stars appear to have detectable planets, half of the stars with planets appear to have multiple planets, and planets with longer periods – such as our Jupiter - are starting to be found. Within the last year, gas giant planets have been observed with orbital radii similar to Jupiter. In the past few weeks (August 2004) announcements have been made of three planets being found that are likely to be large rocky planets. They are in small rapid orbits close to their stars, so must be extremely hot, but they are a continuation of expansion of our knowledge about what might be out there. All these exciting discoveries lead to the conclusion that planets are likely to be orbiting other stars that could carry life as we know it on Earth.

With this in mind, NASA is funding a mission called Terrestrial Planet Finder (TPF) that intends to find and characterize terrestrial (or rocky) planets that might harbor life. The ability to harbor life is defined as having liquid water present on the planet surface. In order to meet this criterion, the planets must be orbiting in the habitable zone or the spherical region around a star where water will be liquid. This is based on the temperature on the surface of the planet being between 0ºC and 100ºC. The liquid water region around each star is related to the brightness of the star so is defined as a radius range for each particular star where a planet would have the correct thermal characteristics. The radius range is scaled by the luminosity of the star. In our solar system, Venus is too hot, but Earth and Mars are both in the habital zone for our sun. Farther out from Mars, planets are too cold.

When a planet is found, by studying the light from that planet, the presence of life can be detected from the spectrum of gases in the atmosphere that will affect the detected light. This is known because the presence of life on Earth can be detected by studying the light from the sun that reflects off of Earth. The presence of water, CO_2, Methane, and other life-indicating gases can be detected from light reflecting off of Earth's atmosphere. The ability to detect life depends on collecting light from a planet and characterizing the spectrum of the light. This will be done using a spectrometer in the instrument suite of TPF Coronagraph.

The defined science requirements for TPF are: look at roughly 50 stars near earth from a carefully selected list that might provide an environment that could harbor life; detect earth-like planets in the habitable zone with 90% chance of seeing any planets that are there; if an earth-like planet is detected, characterize its atmosphere so that the presence of life can be detected using the spectral range of visible wavelengths from 500 to 800 nm with spectral resolution of 70 divisions through the range (4.3 nm per resolution element); and as a goal, provide information about the other planets and the dust disk that surrounds the star.

In order to perform this mission, two instruments are being proposed: a visible coronagraph and an infrared interferometer. The coronagraph is currently scheduled for launch in 2015 and will be the focus of this talk. The interferometer was the focus of a talk last year at this conference and is currently scheduled to launch in the 2018 timeframe. Both instruments provide complementary data to establish the presence of life on any planets that may be found and studied.

II.   Features of the TPF Coronagraph

The optical system for this mission must be specially designed to be able to search for terrestrial planets. Currently Hubble Space Telescope has perhaps the smoothest surface figure on its large primary mirror of any telescope launched into space; but, if you look at images of stars taken by the Hubble Space Telescope (HST), as illustrated by Fig. 2, you observe spikes of light radiating from the star image. These are caused by light that is diffracted off of

Figure 2. Star image from Hubble Space Telescope

structures in the telescope such as the spider-structure that supports the HST on-axis secondary mirror. In order to detect planets in the habitable zone, the TPF Coronagraph needs to reduce the scattered light from the star to a level that hasn't been done before. The diffraction spikes of Hubble Space Telescope cover any of the faint planets that might occur in the habital zone of the star shown in Fig. 2. To avoid this, the TPF Coronagraph optical telescope

will be an off-axis Cassegrain design that will have no diffraction contribution from structure supporting the secondary mirror. Fig. 3 shows a plot of the simulated fall-off of star intensity versus radius from the center of the star with the TPF Coronagraph type of design. It represents the performance of an off-axis telescope with optics as smooth as Hubble Space Telescope. Curve (a) shows how the star light diminishes as the radius from the star increases; curve (b) shows the star light suppression if a coronagraph is added to the telescope to block the star light; and curve (c) shows the star light suppression if a coronagraph and active wave front sensing and correction are added to the telescope to correct residual errors from the mirror surfaces of the telescope.

Fig. 4 is a repeat of curve (c) from Fig. 3 with representative planets overlaid at the brightness and radii at which they would appear. The Earth is represented as the second planet from the star – shown at Earth's actual radius and brightness. This illustrates that Earth's image is the same intensity as background light that is residual from the star
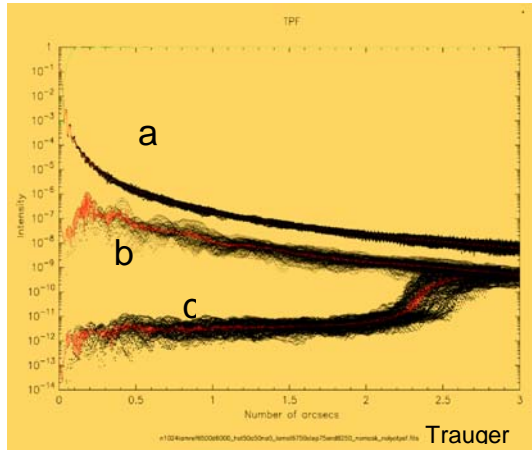

Figure 3. Star intensity versus radius: *(a) TPF Coronagraph type telescope with HST-smooth optics; (b)Coronagraph added; and (c)actively corrected and coronagraph.*
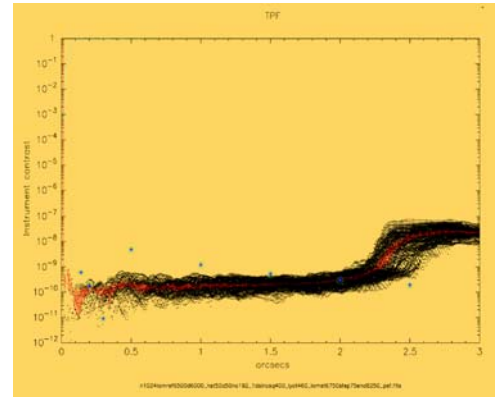

Figure 4.   TPF Instrument PSF (c): *Overlay: an exo-planetary system at 5 pc with Venus, Earth, Mars and Jupiters at 2.5, 5.0, 7.5, 10.0, and 12.5 AU respectively from left to right.*

even after a coronagraph with wave front sensing and control have been applied. A target planet will likely have the same intensity as the background. Fortunately, there are techniques for subtracting background light that is caused by the telescope and its diffraction and mirror surface scatter. By rolling the telescope, all artifacts caused by it will roll, too. The planet will be stationary. By subtracting images, the planet can be detected.

The two additions to the telescope that are shown in Fig. 3 are a coronagraph and wave front sensing and control. Fig. 5 shows a schematic of this complete system. It consists of a telescope – off-axis Cassegrain, a fold mirror, and then a collimating mirror that sends the beam into a polarizing beam splitter. The two polarization states of the light are split apart because they will smear the light at the science camera focal plane if they are not corrected separately. Looking at one of the split beams, the light then enters a Michaelson Interferometer which splits the beam into two paths that later are recombined. Each path is necessary for complete beam correction. In each path, a deformable mirror can adjust to correct the wavefront. Both mirrors are necessary to adjust a flat wavefront in both phase and amplitude of the light. When the beam is recombined, it has been corrected for errors that exist on the telescope mirrors and for non-uniformity in the coatings on the mirrors. This nearly-perfect wavefront is then relayed to a pupil plane where a mask is inserted to block star light. The pupil plane masks diffract the starlight away from the field of the habitable zone. The light is then focused and at the focal plane, an occulting mask is inserted to block the central starlight that passes through. The next step is to re-collimate the beam which will kick any diffracted light out to the edges of the field. This ring of light is blocked by a Lyot stop. Finally, the beam is relayed into a focus mirror which images it onto the science camera. After the telescope is rolled, the residual background light can be subtracted and the camera will see an image similar to what is shown. The square shaped dark hole is created because of the square shape of the deformable mirrors. If they were round, the dark hole would be round. In the dark hole, planets can be seen outside of the star light that has not been eliminated totally.

This concept for creating an area of starlight suppression that encompasses the habitable zone of the target stars is being demonstrated in a testbed that is being developed by NASA at Jet Propulsion Laboratory. The telescope
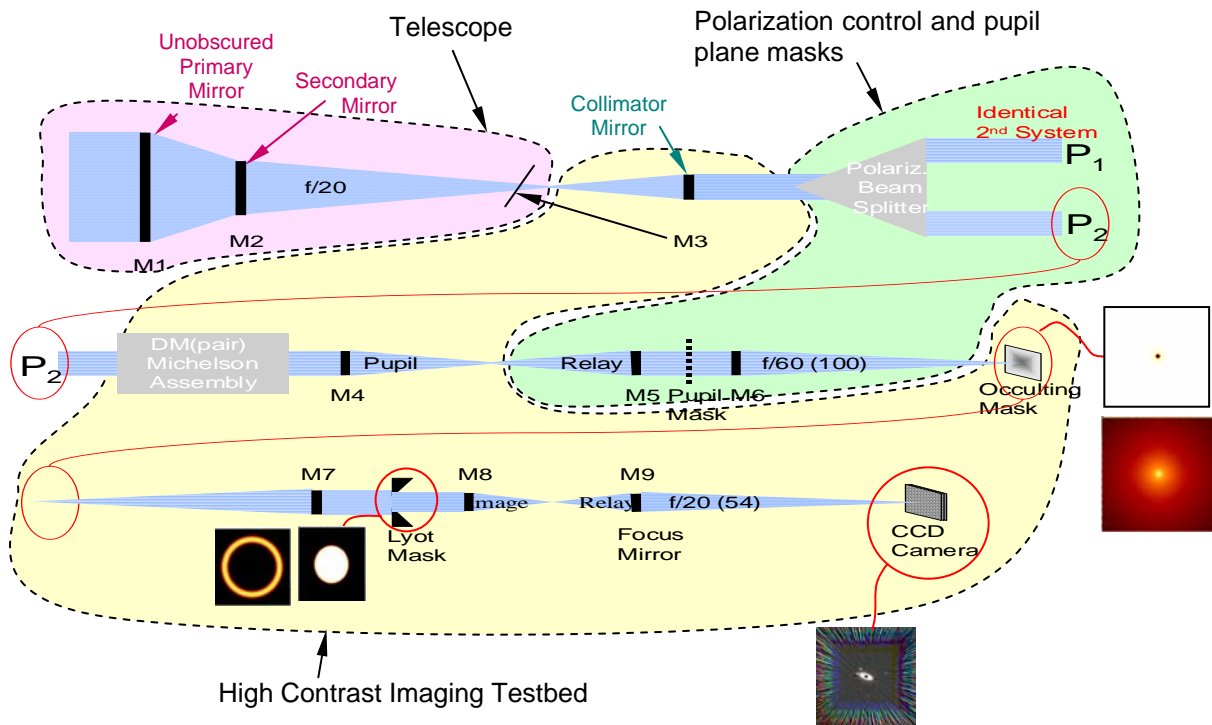

Figure 5. TPF Coronagraph Optical Schematic

Figure 6. High Contrast Imaging Testbed. Remote Guest Testing in progress, Contrast Results to date: 1.5x10e-9

Figure 7. Mask types for Coronagraph

shown in the schematic is currently replaced by a fiber optic source followed by a pin hole that delivers a beam representing a star. This is injected at the first focus shown in the schematic. The current components of the test bed are enclosed by the dotted line labeled High Contrast Imaging Testbed (HCIT). Components that are planned to be added to the test bed are enclosed by the line labeled Polarization control and pupil plane masks. The HCIT, shown in Fig. 6, is where the advanced technologies needed for this mission are studied, tested, and explored. Currently the testbed is evaluating occulting masks, deformable mirrors, control electronics, and wave front sensing
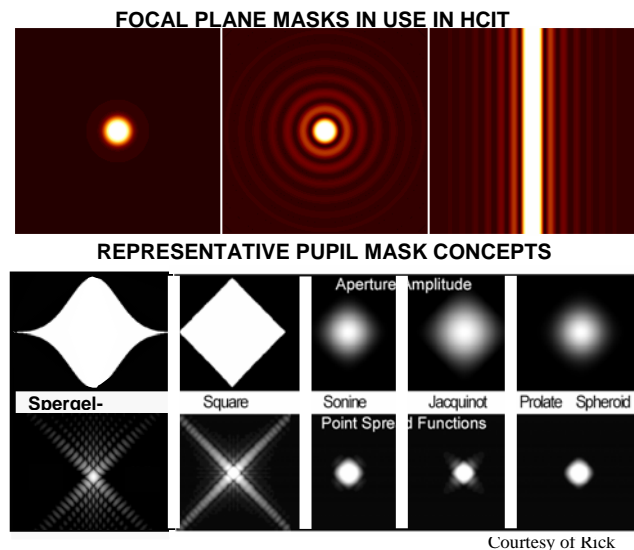
and control algorithms to produce a dark hole around the source spot in the science camera plane. Different varieties of masks will be tested, with results being used to understand the modeling used to create the masks, and to refine the designs and the tolerances that constrain the mask fabrication. A picture of a variety of masks is shown in Fig. 7.

The deformable mirrors being used have been under development at Xinetics Inc. for nearly 10 years and are very stable, high actuator density devices based on electrostrictive material technology. Further refinements will bring them closer to being ready to survive the environmental loads of space flight. Fig. 8 shows two deformable mirrors – a 32x32 actuator version and a 64x64 actuator version. Electrical interconnects, drivers and the algorithms that sense the wavefront and calculate the optimal deformable mirror shape have been developed to produce a system with nearly good enough capability.

The current level of contrast between the incoming source and the dark hole at the science camera that has been achieved in the HCIT is $1.5x10^{-9}$ as shown in Fig. 9. The contrast needed to sense terrestrial planets is calculat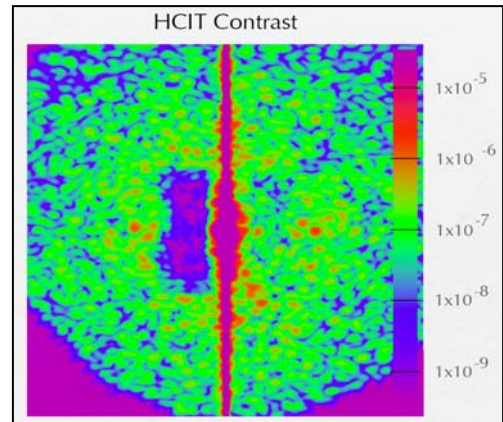ed to be $1x10^{-10}$, so there is still a factor of 10 needed to meet the required performance. In addition, the contrast shown was achieved with a laser at wavelength 785nm. When the waveband is expanded, the contrast degrades to 10^{-8}. The test bed team is working toward better broad band performance and a factor of ten improvement in contrast. In addition, they will be exploring different types of masks such as pupil plane forms that are being developed at Princeton University. Deformable mirror refinements, source improvement, algorithm development and wavefront sensing improvement are also being explored.

Figure 8. Deformable Mirrors, Xinetics, Inc. *64x64 actuator model*

Figure 9. Science Camera picture showing contrast between source and dark hole of 1.5x 10⁻⁹ achieved in the HCIT. *Trauger and Burrows, May 2004.*
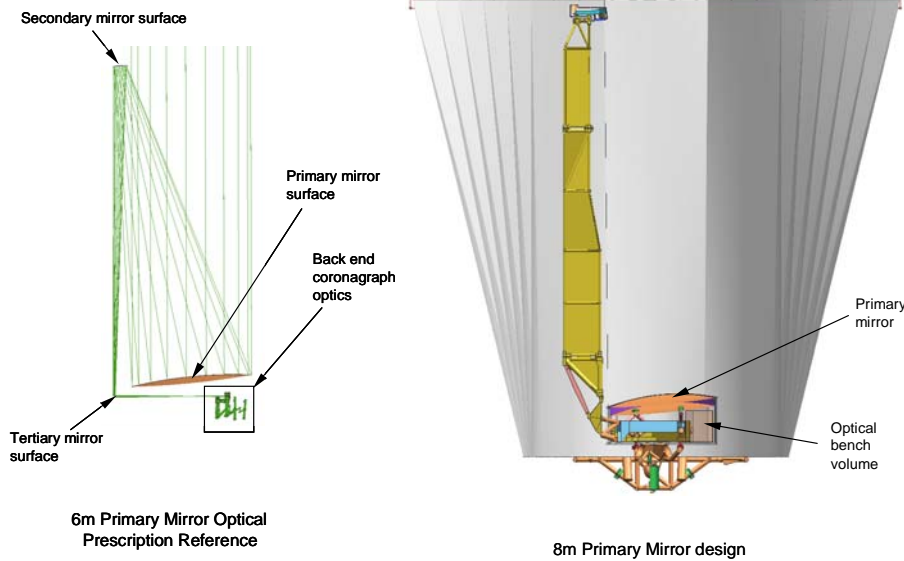

6m Primary Mirror Optical Prescription Reference

8m Primary Mirror design

Figure 10. Optical Design and Accommodation.

III.   TPF Coronagraph Mission Configuration

The first design study featured an off-axis cassegrain telescope with a 6 meter by 3.5 meter primary mirror. Currently a flight baseline is being developed that is likely to be a scaled up version to an 8 meter by 3.5 meter

primary mirror. This is because the tolerances for position of the mirrors is loosened for the larger mirror system. An optical ray and system picture showing these two mission configurations is shown in Fig. 10. The starlight enters the telescope through the center of the radiator, reflects off the primary mirror and converges towards the secondary mirror. It is then focused into the back-end coronagraph optics.

The system is protected from the sun with a 6 vane v-groove radiator. This radiator rejects the heat from the sun so that the telescope can rotate about its observing axis without significant deformation of the wavefront. Extreme thermal stability is required so the optical wavefront will remain stable enough to allow for subtraction of the diffraction speckles created by the telescope. The v-groove radiator is based on technology developed for a deployable v-groove radiator for James Webb Space Telescope. The radiator must be deployed in space because it will not fit into a launch vehicle. The deployment is very challenging, requiring both radial and axial motion, tensioning the thin vanes, and stowing behind the primary mirror in the launch configuration. Currently, a feasibility study by Astro Aerospace of Northrop Grumman Space Technology has produced the sun shade deployment concept shown in Fig. 11.

Some details of the system design are shown in Fig. 12. The back of the primary mirror is surrounded by a heated thermal enclosure that maintains a steady, controlled temperature gradient through the primary mirror, the
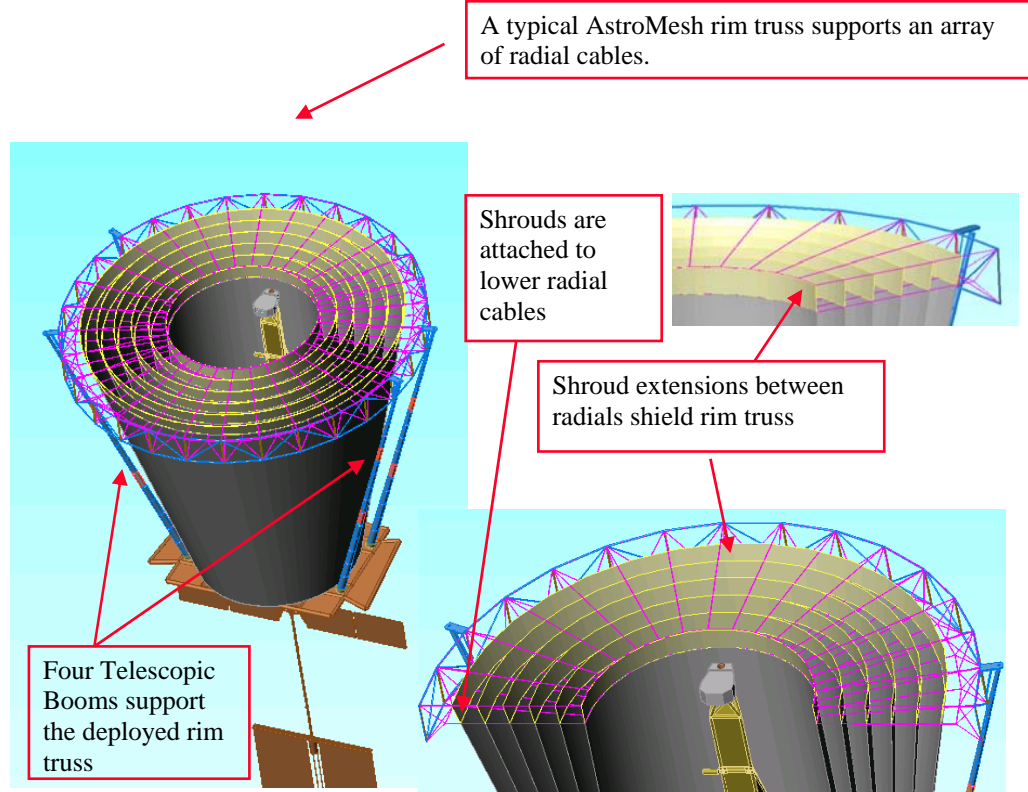

A typical AstroMesh rim truss supports an array of radial cables.

Shrouds are attached to lower radial cables

Shroud extensions between radials shield rim truss

Four Telescopic Booms support the deployed rim truss

Figure 11. Sun shade feasibility study by Astro Aerospace, Northrup Grumman
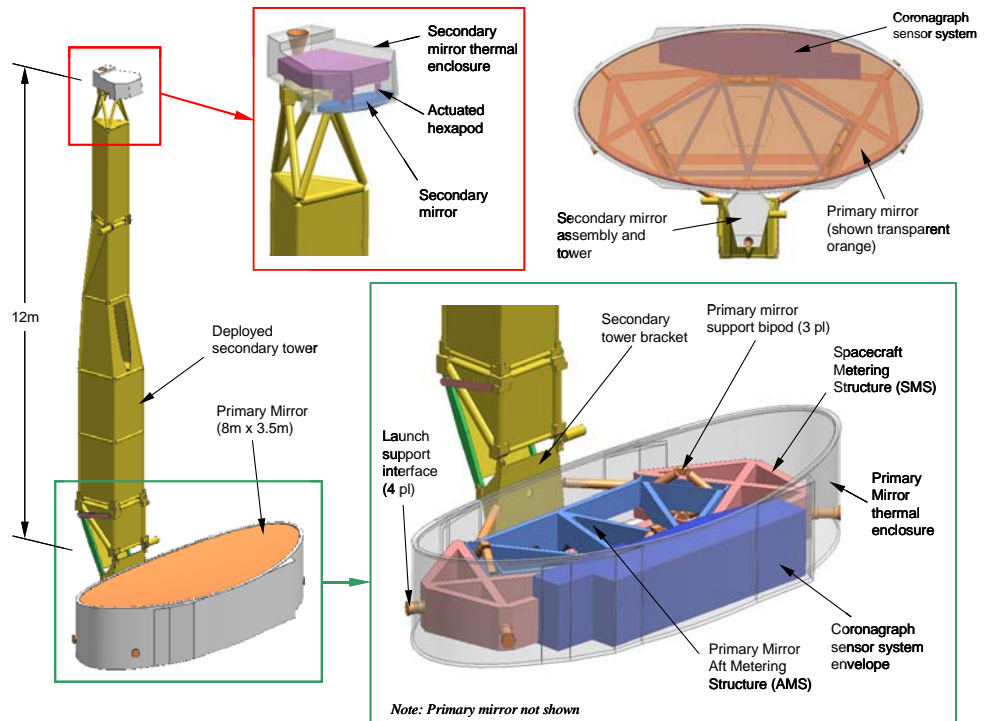

Figure 12. Payload Assembly

coronagraph, and the science instruments. The temperature will be close to room temperature to allow the primary mirror to operate at the same temperature that it is fabricate in. There is a similar smaller enclosure around the secondary mirror that keeps its temperature steady at room temperature.

Behind the secondary mirror is an actuated hexapod with dual stage actuators that provide both coarse and fine position adjustment. The design is based on actuators being developed for James Webb Space Telescope. The support for the actuated hexapod is thermally isolated from the secondary tower. The secondary mirror and primary mirror will have a 6-beam laser metrology system that will permit positional monitoring of the secondary mirror relative to the primary mirror at all times. This system is similar to the laser metrology systems currently being developed for Space Interferometer Mission and the Laser Interferometer Space Antenna.
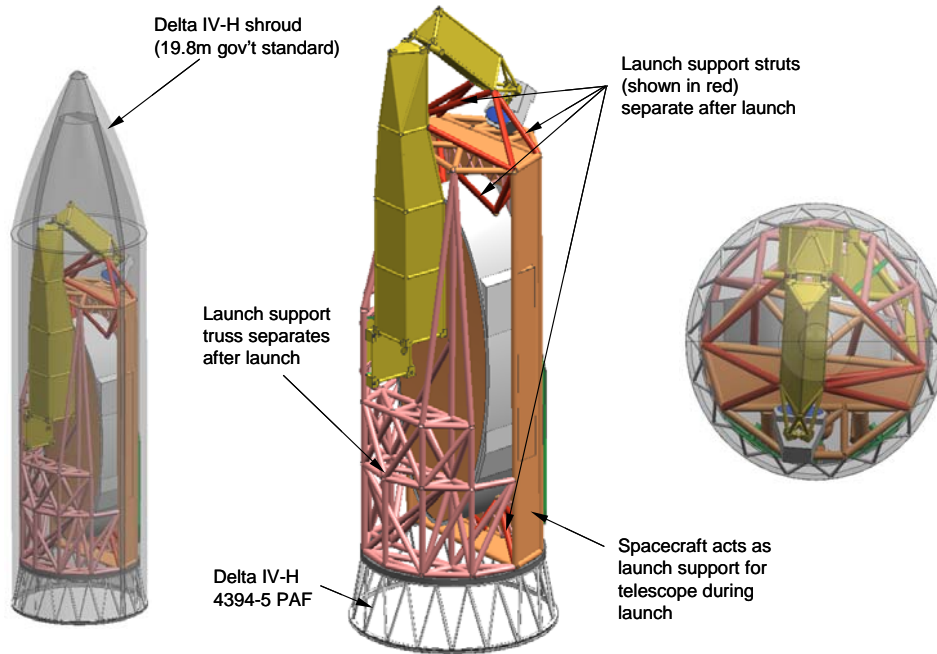

Figure 13. Stowed Flight System.

The secondary tower itself will not be thermally controlled. At the base of the tower, a fold mirror directs the optical beam into the thermal enclosure towards the coronagraph and other science instruments. The tower is attached to an aft metering structure through three thermally-isolating bipods. The aft metering structure supports the telescope components – the primary mirror and the secondary tower. It is supported to a payload support structure that integrates the telescope to the instruments. The payload support structure attaches to the spacecraft through thermal and dynamic isolators.

The spacecraft contains the computer, the power system, the thrusters, propulsion tanks, reaction wheels and the telecom system. A deployable shaft supports solar panels and a long solar sail that balances the solar pressure of the system. The sun shade is supported from the space craft as well.

Two orbits are being considered for the mission: an Earth drift-away orbit like Spitzer Infra Red Telescope or the L2 point semi-stable orbit like James Webb Space Telescope. Both orbits have similar environments, but have different requirements for quantities of fuel required and telecom systems.

The system must fold up to fit within the launch vehicle shroud. Fig. 13 shows the folded configuration. The launch vehicle selected is the Delta IV-Heavy – the largest that is currently available. The system folds up with parts latched to structure that is jettisoned after launch.

IV.   Modeling and Analysis

The goal of the pre-Phase A design team has been to develop, model, and analyze a design that meets the tight requirements for terrestrial planet finding. Several levels of models have been developed – a coronagraph performance model; an optical sensitivity model; structural and thermal models; and dynamics models.

The coronagraph performance model represents the propagation of light through the entire system incorporating diffraction and polarization effects. It produces an image at the science camera plane that includes speckles caused by diffraction, polarization, wavelength shift and aberrations. This image is used to calculate contrast in region where terrestrial planets might appear. This model is being built of the HCIT. Early versions showed loose correlation to measured results. Improvements are being implemented.

The sensitivity model is derived via matrix algebra to capture the impact on wavefront caused by most of the aberrations in the coronagraph system. Each optical element is perturbed in all degrees of freedom by one unit. The resulting degradation in contrast is recorded as a sensitivity term in a perturbation matrix. Both rigid body and flexible optical modes are captured. When an array of perturbations is developed from other models, an aberrated wavefront can be calculated. The wavefront that results is described in terms of the Zernike coefficients.

The structural and thermal models are built using standard commercial software products. The thermal model is linked to the structural model via similar finite element structures. When perturbations are calculated using these models, they are fed into the sensitivity matrix which calculates the resulting wavefront in terms of Zernike coefficients.

The structural model feeds the dynamics model so that the impact of vibrations caused by dynamic perturbations during an observation can be calculated. The vibrations that have been analyzed are caused by the reaction wheel assemblies. Existing assemblies were used to derive the input vibration loads. The model has been developed to include passive vibration techniques and active vibration techniques. Lockheed Martin has provided the active vibration isolation modeling for this feasibility study.

The performance model and the sensitivity model have been used to develop an error budget. The structural, thermal and dynamic models have been used to calculate perturbation magnitudes which are fed into the sensitivity matrix to derive resulting wavefront aberrations. These are compared to the error budget to determine whether the requirements for TPF coronagraph science are met.

V. Analysis Results

Only the first system that was designed has been fully modeled and analyzed. This system was called the Minimum Mission Design. It aimed at meeting the minimum science requirements – mostly related to the distance that stars could be searched for terrestrial planets. The farther stars require a bigger primary mirror to see with tight enough resolution at a smaller angle from the star. The Minimum Mission Design was based heavily on a precursor study done by Ball Aerospace Corporation and consists of an off-axis cassegrain system and a 6 meter x 3.5 meter primary mirror. The full design is pictured in Fig. 10. The details of the Minimum Mission Design are shown in Fig. 14.

The analysis was based on an assumed operation scenario as follows: Every target star will be visited 9 times over 3 years; each observation consists of: 1) Acquire star, stabilize, set deformable mirror and observe 2) Rotate 20º about Line-of-Sight (LOS), adjust secondary mirror to within 1 nm of best position, observe 3) Difference the
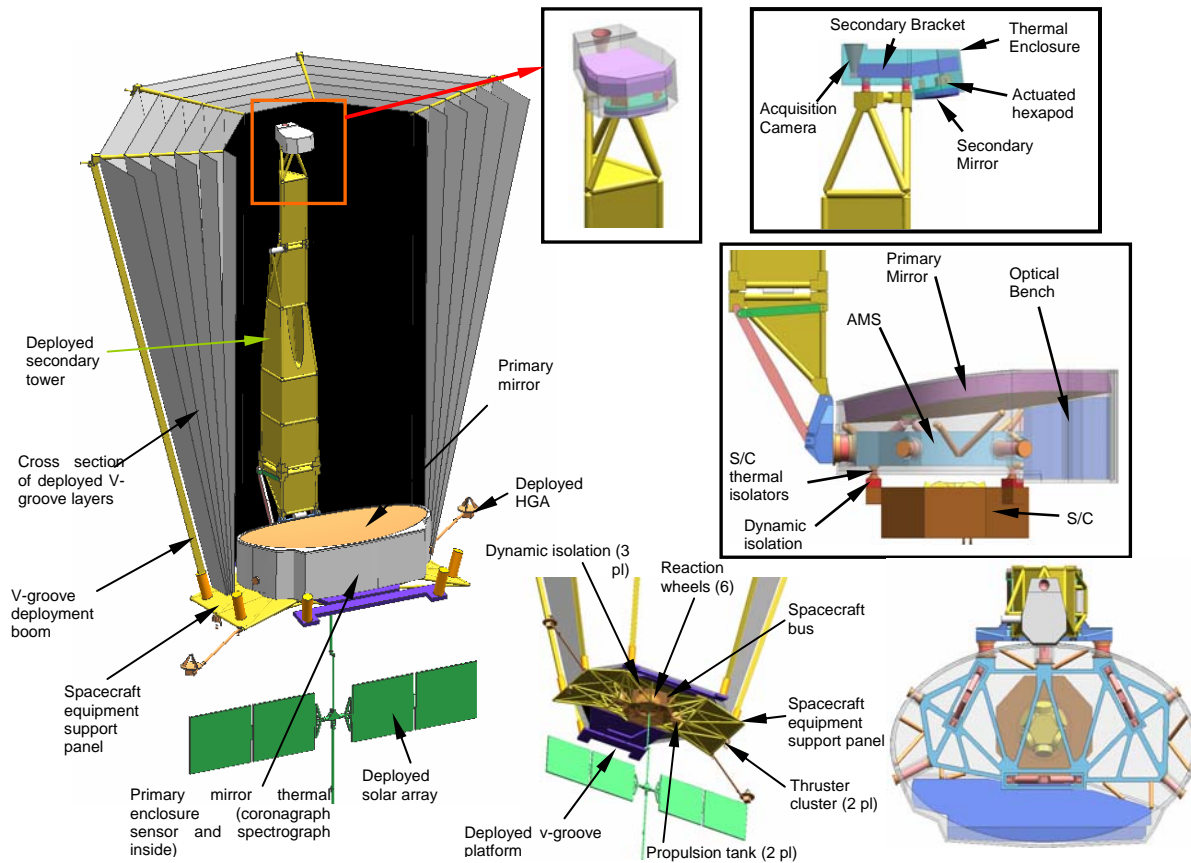

Figure 14. Minimum Mission Design Concept

images 4) Rotate 70º about LOS, stabilize, set deformable mirror and observe 5) Rotate an additional 20º about Line-of-Sight (LOS), adjust secondary mirror to within 1 nm of best position, observe 6) Difference the images. The analysis was based on this sequence and looked at the perturbations that were created by the 20º rotations in steps 2 and 5 because these rotations do not have a reset of the deformable mirror between them.

Additional assumptions were: No calibration of dynamic/thermal wave front changes; Speckles look like planets, no chromatic differentiation; Deformable Mirror is set and forget between dithers, leading to Static Wave Front Budget; 7 classes of optic are used for beam-walk calculations: primary, secondary, DM, small flat, small power, super flat, and super off-axis paraboloids; Near field diffraction effects are ignored (deformable mirror can correct much of this); and Errors are uncorrelated so contrast contributions add linearly.

A. Thermal Modeling Results

The thermal analysis of the Minimum Mission Design concentrated on the impact of the changing position of the system to the sun. The telescope will be restricted to looking at stars that are in the semi-hemisphere of the sky away from the sun. With this restriction, the worst case solar conditions are experienced when the sun is 90 degrees from the line of sight of the telescope. In this condition, the sunlight hits the maximum area of the sun shade. The analysis performed evaluated the conditions with the sun in this maximum impact position, and calculated the thermal change between the operational conditions when the telescope was required to be most stable – steps 2 and 5. These two steps are shown in Fig. 15 in the upper left corner where the sun is shown at positions separated by 20 degrees. These figures also illustrate the spacecraft coordinate system, since the position and angle designation of the sun are shown. The two steps are orthogonal to each other so that the long axis of the telescope (or highest resolution direction) will line up to cover the full area around the star. The top right of Fig. 15 shows the telescope
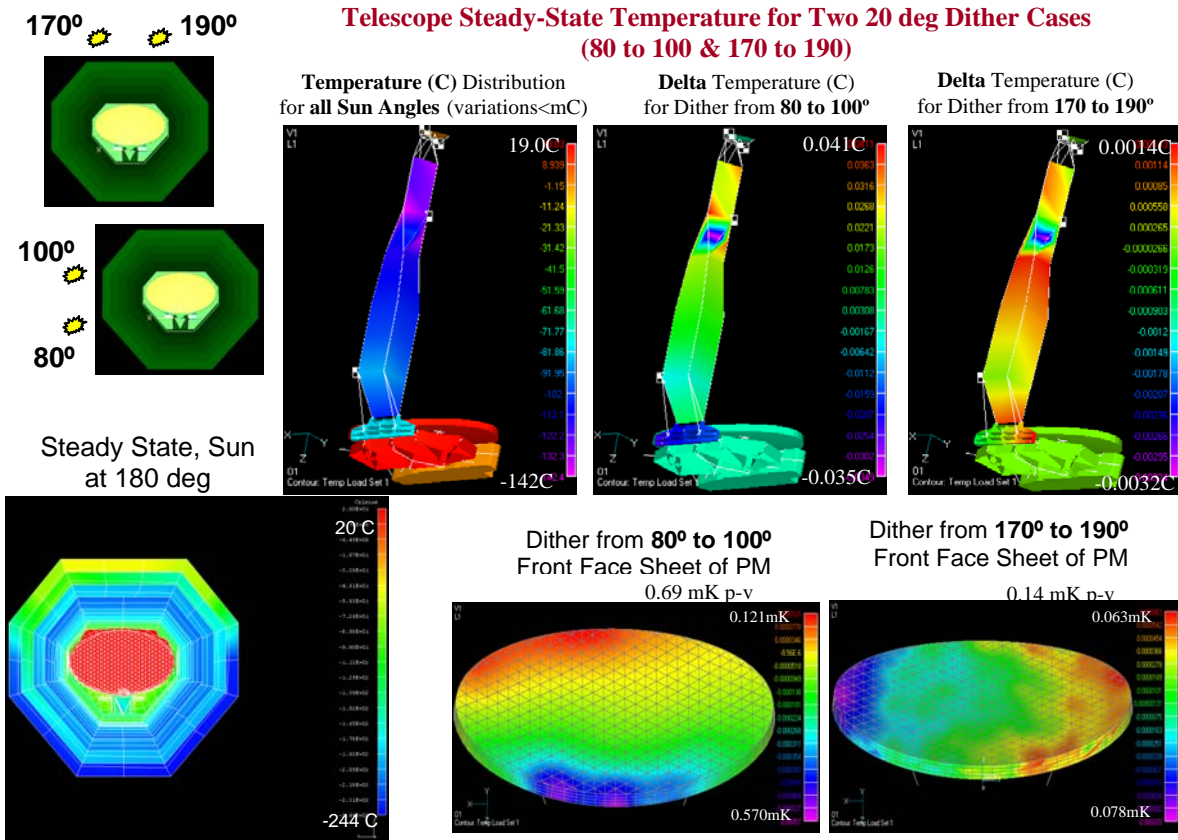
Telescope Steady-State Temperature for Two 20 deg Dither Cases (80 to 100 & 170 to 190)

170⁰   190⁰

100⁰

80⁰

Steady State, Sun at 180 deg

Temperature (C) Distribution for **all Sun Angles** (variations<mC)

Delta Temperature (C) for Dither from **80 to 100º**

Delta Temperature (C) for Dither from **170 to 190º**

Dither from **80º to 100º** Front Face Sheet of PM
0.69 mK p-v

Dither from **170º to 190º** Front Face Sheet of PM
0.14 mK p-v

**Figure 15. Minimum Mission Design Thermal Analysis**

temperature scenarios from left to right: the average temperature distribution for all sun angles; the change in temperature of the telescope going from sun positioned from 80 to 100 degrees relative to the spacecraft coordinate system; and at the right, from 170 to 190 degrees relative to the spacecraft coordinate system.

The lower left image shows the system looking down into the sun shade at the primary mirror. The primary mirror is actively heated to be close to 20 degrees C. The sunlight is hitting the shade from the top of the image. The shade is warmer on that side. Going inward, the shade cools to a uniform temperature all the way around, then warms as the inner layers are heated by the primary mirror.

The two figures on the lower right of Fig. 15 show the thermal change in the front face sheet of the primary mirror between the two steady state conditions before the indicated change and after it. Note the temperature difference range for each figure. For the 80 to 100 degree case, the maximum temperature change across the primary mirror front face sheet is 0.69 milli Kelvin. For the other case, the maximum temperature change is 0.14 milli Kelvin.

The impact of the thermal change on the wavefront is shown in Fig. 16. The primary mirror is made up of 21 hexagonal segments that are fused together as shown in the top center of Figure 16. Each segment is made of a core and two face sheets that are fused together to make a light weight section. Each section will have a slightly different coefficient of thermal expansion for its core and its front and back face sheets. In this analysis, the ranges of possible combinations of coefficients of thermal expansion are distributed using Monte Carlo analysis. The segments are placed in the optimum position for its particular set of properties. This can be done as the final primary mirror is fabricated since the glass properties can be measured and selected for each location.

Using this technique, and the thermal results, the two tables in Fig. 16 were generated. Each table describes the wavefront change produced by the thermal gradient that was calculated and described in Fig. 15. In the left column of each table, each row is identified by the Zernike coefficient that describes the wavefront. The second column shows the value of the Zernike coefficient in picometers that is generated by the mirror response to the induced

<div>
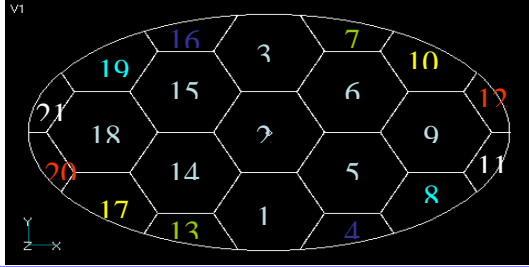
Summary for PM Design with **Optimized** Segment Placement Based on 80 to 100 deg Dither				Results for 170 to 190 deg Dither Using **Optimized** Segment Placement			

	80 to 100 deg Dither				170 to 190 deg Dither		
Zernike Comp	Stead-State Resp (pm)	3L/D Req Specs (pm)	Ratio Req/Resp	Zernike Comp	Stead-State Resp (pm)	3L/D Req Specs (pm)	Ratio Req/Resp
4	0.14	2.29	16.21	4	0.02	2.29	126.52
7	0.19	0.29	1.47	7	0.06	0.29	4.88
11	0.09	0.14	1.64	11	0.01	0.14	22.70
12	0.11	0.29	2.53	12	0.01	0.29	40.28
13	0.07	0.29	3.86	13	0.03	0.29	9.93

Note: The results for PM with optimal segment placement are **steady-state** (conservative for dither)

</div>

Figure 16. Analysis of Minimum Mission Design Results

thermal change. The third column shows the allowed error in picometers in the Zernike coefficient that is allocated for thermal response. The fourth column shows the ratio of allowed error divided by the calculated response (column 3 divided by column 2). If the value in the fourth column is above 1, then the performance is meeting the requirement. With the optimized placement of segments, the mirror does demonstrate acceptable thermal response to the operational motions.

B. Structural and Dynamic Modeling, Analysis and Results

A structural model was developed of the full TPF Coronagraph system as shown in Fig. 17. The spacecraft, the telescope, the coronagraph component assembly, the solar panels, the sun shade, and the solar sail were included in the model.

The primary mirror was modeled with a medium fidelity grid and portions with a high fidelity grid. The results were compared between the two regions and showed negligible difference in mirror shape performance.

The structural materials that were assumed are shown in the center of Fig. 18. Standard vendor data was used to define material properties except in cases where better data was available through precision testing.

This model was used to evaluate the thermal response of the system and also the dynamic response of the system to the continuously rotating reaction wheels in the spacecraft. The reaction wheels will be the largest source of vibration causing jitter during observation. Reaction wheel vibration data was used from vendor data as well as measured data available from other projects.

Two layers of passive isolation were assumed for passive damping between the reaction wheels and the payload. The damping characteristics that were used were based on data from other flight missions.

A pointing control system was assumed as shown in the schematic in the bottom center of Fig. 17 with an acquisition camera for coarse alignment mounted on the secondary tower. A fast steering mirror is planned for fine adjustment of pointing.

The resulting wavefront error caused by the reaction wheel vibration is shown in the two charts on the lower left of Fig. 18. The upper chart shows the response of the optics moving rigidly. The lower chart shows the flexible response of the primary mirror. The horizontal axis shows each Zernike coefficient from the fourth through the sixteenth. The vertical axis shows the wavefront response in terms of nanometers for each Zernike coefficient. The solid red line shows the maximum allotted error for each Zernike coefficient. The solid blue line shows the maximum response for each Zernike. The symbol at each Zernike coefficient indicates the frequency in Hertz which caused the maximum response for that Zernike coefficient. For the upper chart, the rigid motions of the optics in response to the reaction wheel vibration all fall within the allowable limit. For the lower chart, the response does go higher than the limit for the 8th Zernike coefficient at a frequency of 3 Hertz. This problem can be avoided by running the reaction wheels above 3 Hertz during observation. The analysis indicates the feasibility of designing an isolation system that will enable the TPF Coronagraph to perform its mission.
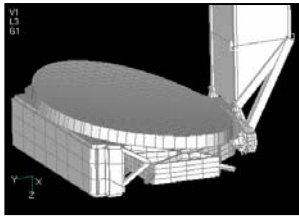
Dynamic Vibration Input:
Reaction Wheel Assemblies with two layers of passive vibration isolation
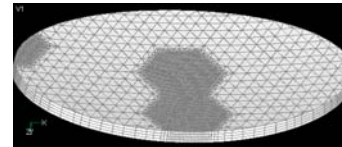
Materials Used:
ULE Glass (Ultra-Low Expansion Titanium Silicate Glass by Corning)
- Primary & Secondary Mirrors (good thermal stability)
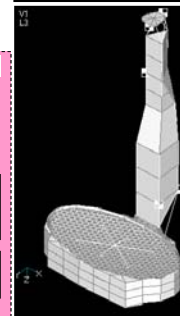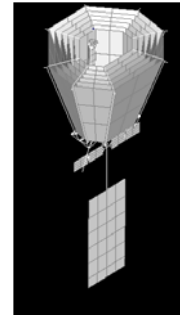
K1100/954 Carbon Fiber Composite
- Primary & Secondary Mirror Thermal Enclosures (high conductivity)

S-Glass Fiberglass Composite
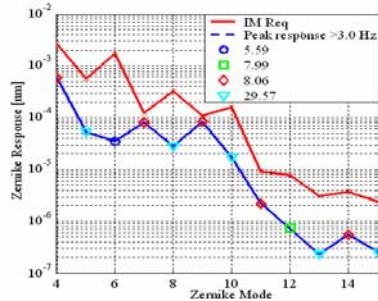- AMS/secondary tower bracket & SMA isolators, launch struts (low conductivity)

M55J/954 GrEp
- AMS, secondary tower & bracket (good thermal stability & stiffness)

Dynamic Results - 2 stage passive isolation

Rigid Optics Wavefront Error

Design meets requirements passively

Flexible Primary Wavefront Error

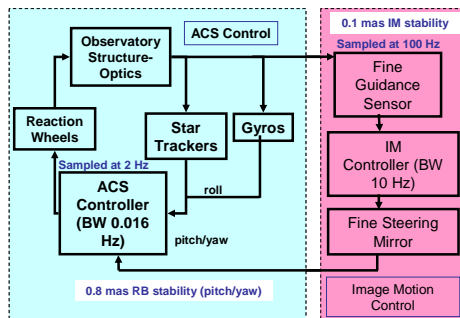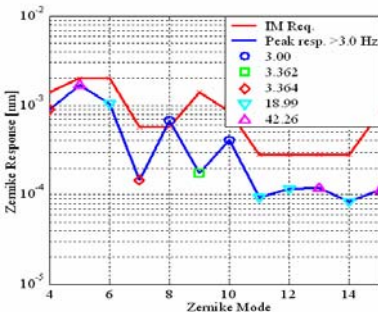Mode 8 exceedance can be avoided by running wheels above 4hz

IM Req
Peak response >3.0 Hz
5.59
7.99
8.06
29.57

Zernike Response [nm]
Zernike Mode

IM Req.
Peak resp. >3.0 Hz
3.00
3.362
3.364
18.99
42.26

Observatory Structure-Optics
ACS Control
Reaction Wheels
Star Trackers
Gyros
ACS Controller (BW 0.016 Hz)
roll
pitch/yaw
Sampled at 2 Hz
0.8 mas RB stability (pitch/yaw)

0.1 mas IM stability
Sampled at 100 Hz
Fine Guidance Sensor
IM Controller (BW 10 Hz)
Fine Steering Mirror
Image Motion Control

Figure 17. Minimum Mission Design Structural and Dynamic Modeling and Analysis

VI.   Conclusion

The goal of this study was to understand whether an environment could be produced which is stable enough to image and characterize light from planets around other stars that might carry life. These preliminary results are promising and indicate that with advanced techniques such as wavefront sensing and control, state-of -the art mirror fabrication, laser position metrology, and advanced mask fabrication techniques, such a mission is feasible. We are entering a time when extreme optomechanical tolerances will be required to perform the missions that enhance astrophysics. We have demonstrated with commercially available modeling techniques that it is possibly feasible to achieve the stability required, but further study is needed to address this realm of extreme high precision. Materials property data measured with great precision is required for inputting realistic values into the models that are built. Current data on materials properties to the precision needed and on extreme precision structural response and stress relief have not been measured to the levels needed. In addition, modeling tool errors will affect the calculated results, so models will need to be verified with testbeds. Because the stable environment required to produce a wavefront that is perfect enough to suppress the starlight for finding planets will not likely be achievable for the large telescope structure during ground testing, validated modeling and source data will be crucial for predicting performance capabilities.

The science goal of possibly finding a life-bearing planet is exciting and significantly appealing. The technology that exists now appears capable of achieving this mission.

Acknowledgments

Center, Lockheed Martin, Northrop Grumman Space Technology, MIDE Technology Corporation, and TC Technology, as well as employees of Jet Propulsion Laboratory.